Fast nonlinear ion transport via field-induced hydrodynamic slip in sub-20nm hydrophilic nanofluidic channels

Udi Vermesh, Jang Wook Choi, Ophir Vermesh, Rong Fan, John Nagarah, James R. Heath

Supplementary Information

Nanochannel Fabrication and Measurement

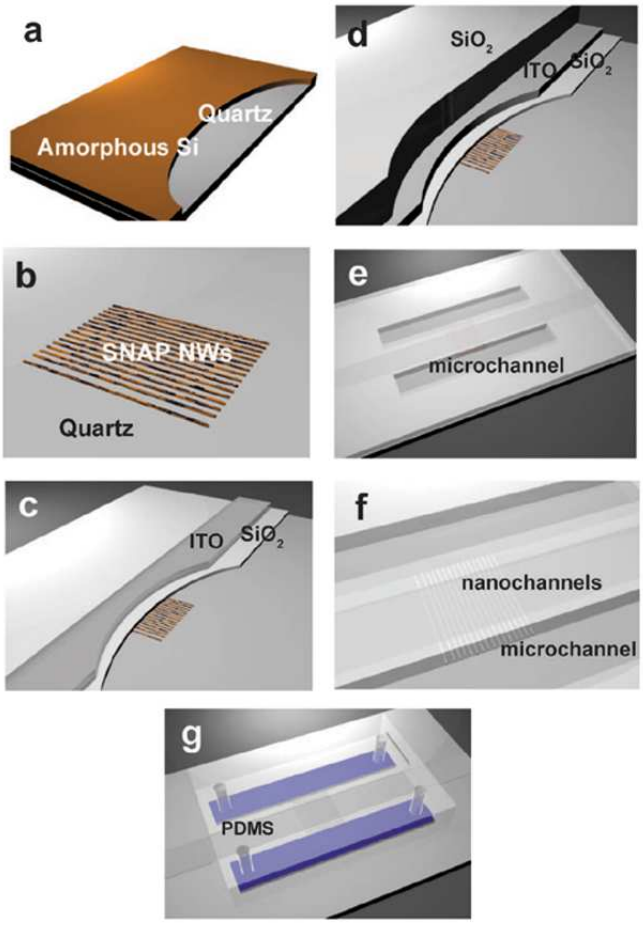

Supplementary Figure 1. Nanochannel device fabrication. **a.** 1 x 1 inch quartz wafer with a 30 nm thick amorphous silicon layer. **b.** A 5um wide array of 80 SNAP nanowires patterned from the amorphous silicon layer. **c.** A 40 nm thick low temperature oxide gate oxide layer is deposited onto the nanowire array followed by deposition and patterning of an indium tin oxide gate electrode. **d.** A 5.5 μm thick low temperature oxide layer is deposited next. **e.** Microchannels are etched through the low temperature oxide all the way down to the level of the nanowires. **f.** Nanochannels are created by XeF_2 etching of the silicon nanowires. **g.** A PDMS slab with input and output holes is aligned over the microchannels and plasma bonded to the wafer. Ionic solutions and Ag/AgCl electrodes are inserted into microchannel inputs on both sides of the nanochannels.

The first step in building nanochannels (Supplementary Fig. 1) was to generate a nanowire template. The SNAP method[21] and standard electron beam lithography (EBL) were used to make an array of silicon nanowires on a transparent quartz substrate with a 30 nm-thick amorphous silicon layer deposited using an e-beam evaporator. In the silicon nanowire array generated by the SNAP method, each wire was about 15 – 20 nm-wide with a pitch of 50 nm. The wires were sectioned into regions 20 μm in length and 5 μm in width

by standard electron beam lithography (EBL). Low Pressure Chemical Vapor Deposition (LPCVD) was then used to deposit a 40 nm-thick silicon dioxide gate oxide layer on top of and between the wires according to the reaction: $SiH_4 + O_2 \rightarrow SiO_2 + 2H_2$. A 50 nm-thick layer of indium tin oxide (ITO) was sputtered on top of the low temperature oxide (LTO), patterned with photoresist, and etched with a 0.5 M HCl solution to create the gate electrode. A 5 µm-thick layer of LTO was deposited on top of the device. Photoresist was spun onto the LTO layer and a microchannel pattern was made by photolithography. The pattern was etched down via an Active Oxide Etching (AOE) process (CHF_3:C_4F_8:Ar = 33 sccm:7 sccm:10 sccm, 200 W, 10 mTorr, 15 minutes) to expose the ends of the SNAP wires. This gave a set of microchannels connecting either end of the SNAP wires. The microchannel depth was about 5.5 µm as confirmed by a surface profiler (Dektak 150). The photoresist was stripped by acetone, and the substrate was further cleaned by a piranha solution (H_2SO_4: H_2O_2 = 5:1 by volume). At this point, XeF_2 was used to selectively and isotropically etch the silicon wires to form hollow channels within the glass according to the reaction: $2XeF_2 + Si \rightarrow SiF_4(g) + 2Xe(g)$. Before loading substrates into the XeF_2 etching chamber, the substrates were dipped into a buffered oxide etching solution (BOE: NH_4F/HF= 6:1 by volume) for 1 second to remove native oxide layers on the exposed tips of the silicon wires. The pressure of XeF_2 gas was maintained at about 2800 mTorr during the etching procedures. The etching progress was monitored by a color change in the array as viewed by optical microscopy. Finally, PDMS with drilled input/output holes was bonded to the device by using an oxygen plasma technique to create a watertight seal between the microchannels. This seal ensures that the only connection between the microchannels is via the nanochannels. Ionic solutions were inserted through the input holes in the PDMS, and the ionic current measurements were carried out with the use of a source/preamplifier unit (Keithley 2400). Commercially available Ag/AgCl electrode assemblies (E. W. Wright) were used. The ensuing electrokinetic current could be read, thereby allowing the characterization of ionic

transport through the nanochannels.

Conductance Equation Derivation

The contribution of slip to conductance enhancement within a nanochannel of radius comparable to the Debye screening length can be modeled as follows. To maintain electroneutrality, the nanochannel surface charge must equal the counterion charge in the solution. This is expressed as:

$$\mathbf{Q}_{surface} = \mathbf{Q}_{solution} \qquad \text{(eq. S1).}$$

This fundamental equation can be expanded to show its components, which gives:

$$\mathbf{A} \times \sigma = \mathbf{V} \times \mathbf{e} \times (\mathbf{n}_K + \mathbf{n}_{Cl}) \qquad \text{(eq. S2),}$$

where $\mathbf{A}$ is the nanochannel surface area, σ is the surface charge density, $\mathbf{V}$ is the nanochannel volume, $\mathbf{e}$ is the electron charge, and $\mathbf{n}_K$ and $\mathbf{n}_{Cl}$ are the K^+ and Cl^- ion densities, respectively. For $[KCl] \leq 10^{-3}$ M, the interior of the nanochannel is virtually unipolar, made up almost entirely of K^+ ions, so that the term $\mathbf{n}_{Cl}$ becomes negligible. The factor $\mathbf{n}_K + \mathbf{n}_{Cl}$ can then be approximated as the parameter $\mathbf{n}_{cr}$, which is defined as the critical ion density within the nanochannel at which ion transport transitions from bulk-like to a surface charge-governed regime (herein, $\mathbf{n}_{cr}$ is equivalent to a K^+ concentration of ~10^{-3} M). Using these conditions along with eq. S2, the surface charge density (σ) of a single nanochannel for $[KCl]_{bulk} \leq 10^{-3}$ M is estimated as a function of $\mathbf{n}_{cr}$ by

$$\sigma = \frac{\mathbf{V} \times \mathbf{e} \times \mathbf{n}_{cr}}{\mathbf{A}} \qquad \text{(eq. S3),}$$

which gives a value of 0.0006 C/m^2. From the ion density, it is possible to find the current ($\mathbf{I}$) associated with ion transport through a nanochannel, which is approximated as[26]

$$\mathbf{I} = \mathbf{e} \times \mathbf{n} \times \mu \times \mathbf{E} \times \mathbf{S} \qquad \text{(eq. S4),}$$

where $\mathbf{n}$ is the ion density, μ is the K^+ mobility (= 7.6×10^{-8} m^2/(V·s)), $\mathbf{E}$ is the electric field defined by source-drain voltage/nanochannel length ($\mathbf{V}_{SD}/\mathbf{L}$), and $\mathbf{S}$ is the cross-sectional area of the nanochannel. The conductance ($\mathbf{G}$) of the nanochannel array in the surface charge-

governed regime at low source-drain bias is obtained by taking the derivative of the current with respect to source-drain voltage ($\mathbf{V}_{SD}$), treating the ion density ($\mathbf{n}$) as $\mathbf{n}_{cr}$, and using eq. S3 to make the conductance a function of the surface charge density, which gives

$$\mathbf{G} = \mathbf{N} \times 4\,\mu\,\sigma\,(\mathbf{d}/\mathbf{L}) \qquad \text{(eq. S5)},$$

where $\mathbf{d}$ is the nanochannel hydraulic diameter (=24 nm), $\mathbf{L}$ is the nanochannel length (=20 micrometers), and $\mathbf{N}$ is the number of nanochannels (80) in the array To account for enhanced ion transport at high source-drain bias, eq. S5 is modified to

$$\mathbf{G} = \mathbf{N} \times 4\,\mu\,\sigma\,(\mathbf{d}/\mathbf{L})\,(1 + \mathbf{b}/l_{stern}) \qquad \text{(eq. S6)},$$

where $\mathbf{b}$ is the extrapolated slip length, and l_{stern} is the thickness of the Stern layer (~0.3 nm), which is also the distance over which the shear plane moves when shifting from no-slip to slip conditions. The relation shown in eq. S5, $\mathbf{G} = \mathbf{N}\times 4\mu\sigma(\mathbf{d}/\mathbf{L})$, represents electrokinetic conductance through the nanochannels without considering slip ($\mathbf{b} = 0$), as shown in Supplementary Fig. 2. The extra term, $1 + \mathbf{b}/l_{stern}$, presented in eq. S6, represents the conductance enhancement due to slip[1, 2]. For conductance in the zero-slip regime, the measured conductance (~14.4 pS) was almost identical to the value (~16.8 pS) obtained using eqs. S3 and S5.

Mechanical Power Calculations

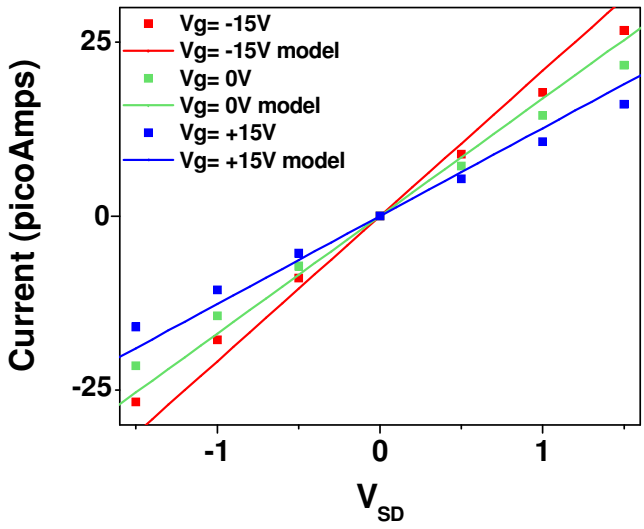

Supplementary Figure 2. Model of gated KCl I_{SD}-V_{SD} curves. I-V curves were obtained for the nanochannel array at low source-drain bias for V_g = -15 V, 0 V, and +15 V. Squares represent experimental data points, and solid lines are based on a calculation of the conductance equation (eq. S5) without the slip-enhancement term so that $\mathbf{b} = 0$.

The mechanical power output of the device - the kinetic energy per unit time associated with electroosmotic movement of fluid through the nanochannel – is defined by:

$$\textbf{Mechanical Power} = \frac{1}{2}(\rho \upsilon_{eof} A)\upsilon_{eof}^2 \qquad \text{(eq. S7)},$$

where υ_{eof} is the electroosmotic flow velocity, ρ is the fluid density, A is the cross-sectional area, and $\rho\upsilon_{eof}A$ is the mass flow rate. To obtain the mechanical power output enhancement from the nanochannel device at high electric fields, we first calculate the electroosmotic flow velocity (υ_{eof}) of a KCl solution with a saturated nanochannel concentration of 10^{-3} M in the low voltage no-slip region and in the absence of a gate voltage by applying the Helmholtz-Smoluchowski equation[27]:

$$\upsilon_{eof} = \frac{\zeta \varepsilon E}{\eta} \qquad \text{(eq. S8)},$$

with η the viscosity of water, ε the permittivity, and E the electric field. ζ is the zeta potential at the shear plane, which can be derived from our previously calculated surface charge density (σ) via the Grahame equation[28]:

$$\sigma^2 = \frac{\varepsilon k_B T}{\pi} n_0 \left[\cosh \frac{e\zeta}{k_B T} - 1\right] \qquad \text{(eq. S9)},$$

where $k_B T$ is the thermal energy, and n_0 is the ion charge density within the nanochannels. This gives an electroosmotic velocity of 3.25×10^{-4} m/s at a source-drain bias of 1 volt. The electroosmotic current (I_{eof}) can be determined from this value by

$$I_{eof} = n_0 \upsilon_{eof} S \qquad \text{(eq. S10)},$$

where S is the cross-sectional area of all 80 nanochannels, resulting in a value of 1.5 picoAmps. This makes up roughly 10 % of the total experimentally measured current of 14.4 picoAmps at 1 volt, although electroosmotic flow has been theoretically shown to contribute up to 25% of ion current in nanochannels[29]. Thus, assuming that electroosmotic

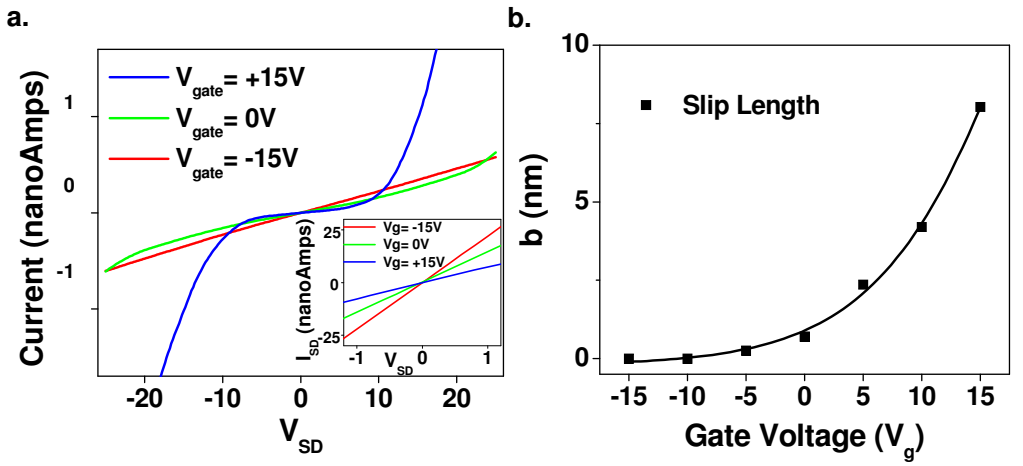

Supplementary Figure 3. The influence of gate voltage (V_g) on the nanofluidic device at [Aspartic Acid] = 10^{-4} M. **a.** Source-drain current (I_{SD}) versus source-drain voltage (V_{SD}) at V_g = -15 V, 0 V, +15 V, with a V_{SD} sweep from -25 V to +25 V. Inset: Expanded I_{SD}-V_{SD} curves illustrating the dependence of conductance on V_g at low source-drain bias. **b.** Dependence of the slip length (**b**) on V_g. The slip length (**b**) increases as V_g is varied from -15 V to +15 V in 5 V increments.

flow accounts for between 10 % and 25 % of the total current, a linear extrapolation of the current from the no-slip, low bias region to higher voltage values results in an electroosmotic velocity of approximately 0.008 – 0.02 m/s at 25 volts. Extracting out the slip-enhanced velocity from the current in the experimental KCl I-V curve with V_g = +15 V shown in Fig. 3 using eq. S10 gives a value of ~1.7 m/s at 25 volts. We assume that electroosmotic flow dominates the current above the slip threshold voltage, so that the velocity value of 1.7 m/s is the electroosmotic velocity. Therefore, fluid velocity is enhanced about 80 – 200 times. We can convert the velocity increases into mechanical power enhancement using eq. S7 above, which shows that mechanical power increases as the cube of the electroosmotic fluid velocity. Comparing slip-enhanced fluid flow to fluid transport confined by the no-slip boundary condition results in a calculated mechanical power output enhancement factor of approximately 5 – 6 orders of magnitude at 25 volts.

Aspartic Acid Measurements

A 10^{-4} M solution of aspartic acid monomers at a pH of 5.5 was inserted into the

nanochannel array, and I-V curves were obtained. The device fabrication and measurement setup were identical to those used in I-V measurements with KCl. The data for the amino acid species under varying gate voltages (Supplementary Fig. 3a) is similar to that seen with 10^{-4} M KCl, with enhanced ion transport occurring above a threshold voltage, but, for aspartic acid, this increase is only observed under the influence of a positive gate voltage. For $V_g = 0$, the conductance is just starting to increase at V_{SD} above $|\pm 20$ V|, and for $V_g < 0$, this phenomenon is completely suppressed at all values of V_{SD}. At low source-drain bias, decreasing conductance with increasing V_g parallels the behavior of KCl (Supplementary Fig. 3a inset) and emphasizes the opposite trend in conductance vs. gate voltage at low and high source-drain bias. The slip lengths range from 0 – 8 nm (Supplementary Fig. 3b), values that are comparable to those seen with KCl, although the suppression of the slip length at negative gate voltages is not seen with KCl under the V_{SD} range measured. However, the similarities between the measurements of the aspartic acid and KCl solutions indicate that positive ions are the dominant charge carriers in the aspartic acid solution. Above a pH of ~3.9, the majority of aspartic acid monomers are deprotonated, giving negatively charged aspartate ions and positive hydronium ions. The negative surface charge of the nanochannels with the ensuing Debye length on the order of the nanochannel radius prevents the entry of aspartate ions, in which case conductance is dominated by hydronium ions. It is interesting to observe increased ion transport above a threshold voltage for this more complex system, showing that this phenomenon may be characteristic of ions in general.

Nanochannel ion conductance (dI_{SD}/dV_{SD}) as a function of [KCl] concentration

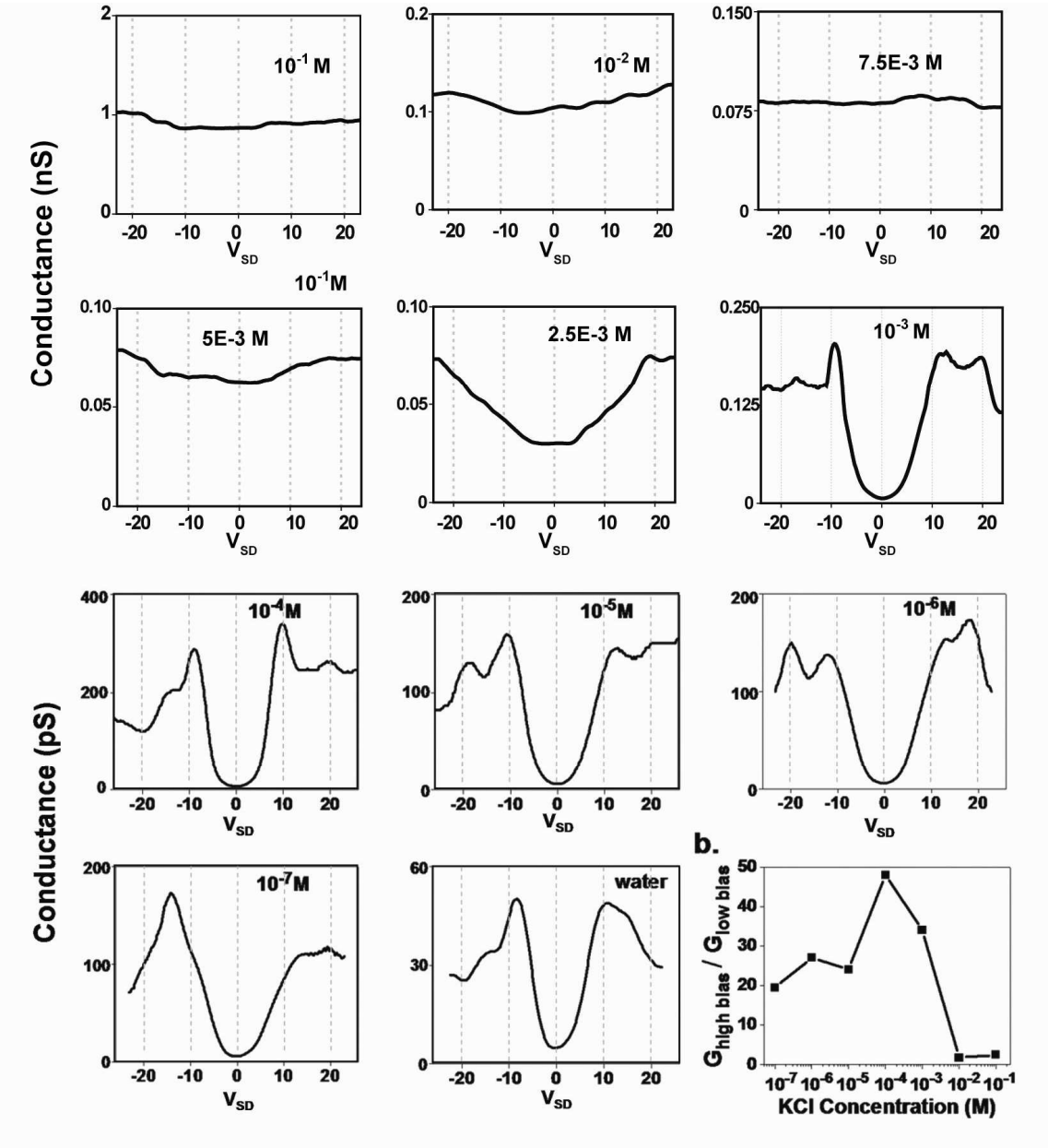

Supplementary Figure 5. KCl conductance plots. a. Differential conductance curves for [KCl] from 10^{-1} M to 10^{-7} M and for water with a V_{SD} sweep from -25 V to +25 V. For [KCl] $\leq 10^{-3}$ M, the conductance plots exhibit a distinctive well shape, reflecting the nonlinear nature of the KCl I-V curves. A first (positive bias) conductance maximum occurs at V_{SD} ~ 8.5 V for [KCl] = 10^{-3} M. As [KCl] is reduced to 10^{-7} M, the well shape broadens, and that conductance maximum shifts gradually to higher voltage. **b.** A plot of the conductance increase versus [KCl]. For this plot, the value of the conductance, averaged over a 1 V range centered at the first conductance maximum, is divided by the conductance at low bias, averaged between -1 V and +1 V. The conductance increases between 20-fold and 50-fold, depending upon [KCl].

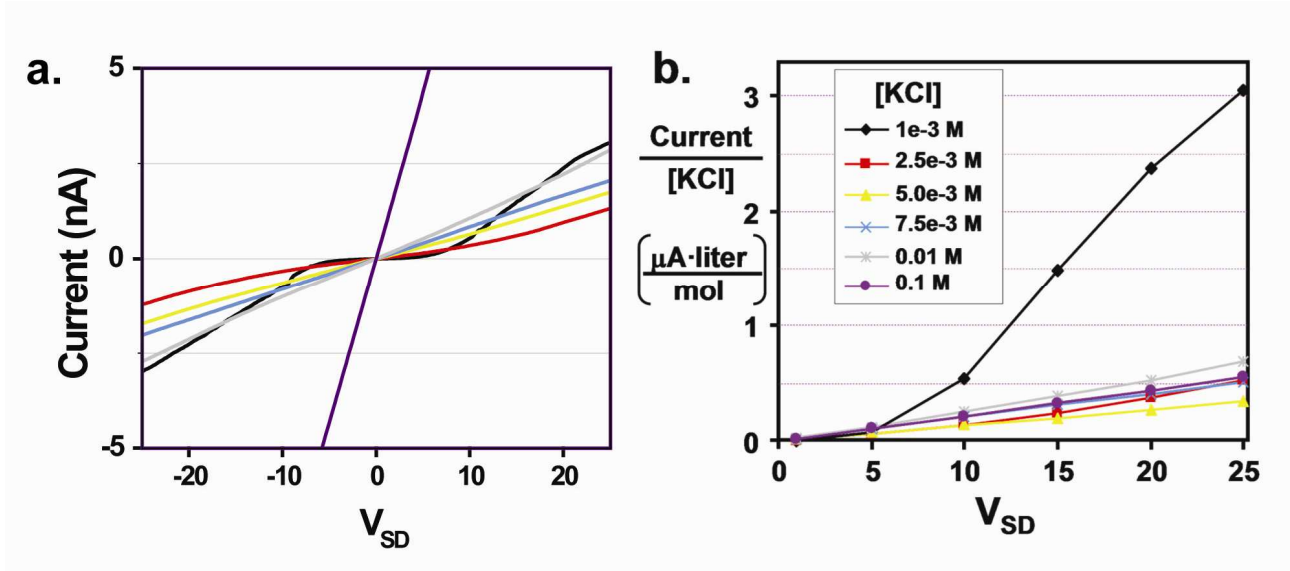

Supplementary Figure 6. Transition from Ohmic flow to saturated current flow. The color code given in panel b applies to both panels. **a.** Source-drain current versus source-drain voltage, as a function of [KCl]. Note the onset of the nonlinear (non-ohmic) response at [KCl] = 10^{-3} M. **b.** [KCl]-normalized source-drain current versus source-drain voltage. This plot reveals that the source-drain current varies approximately linearly with [KCl] to concentrations as low as 2.5×10^{-3} M. Note that, at V_{SD} values > 5V, the concentration-normalized conductance for [KCl] = 10^{-3} M is significantly larger than is observed for the measurements at higher concentrations – a result that is attributed to non-zero slip.

[KCl] (mM)	Concentration Fold Change	Conductance Fold Change
1		
2.5	2.5	2
5	2	2.1
7.5	1.5	1.3
10	1.33	1.4
100	10	9.8

Supplementary Table 1. Measured KCl conductance and concentration fold change factors. (Conductance was averaged over the low bias region centered at V_{SD} = 0 V)**.** The left column displays KCl concentrations from 1 mM to 100 mM with the fold change between adjacent concentrations presented in the middle column. For [KCl] > 2.5 mM, conductance increases roughly linearly with KCl concentration, however, for [KCl] between 1 mM and 2.5 mM, a nonlinear conductance increase is observed.

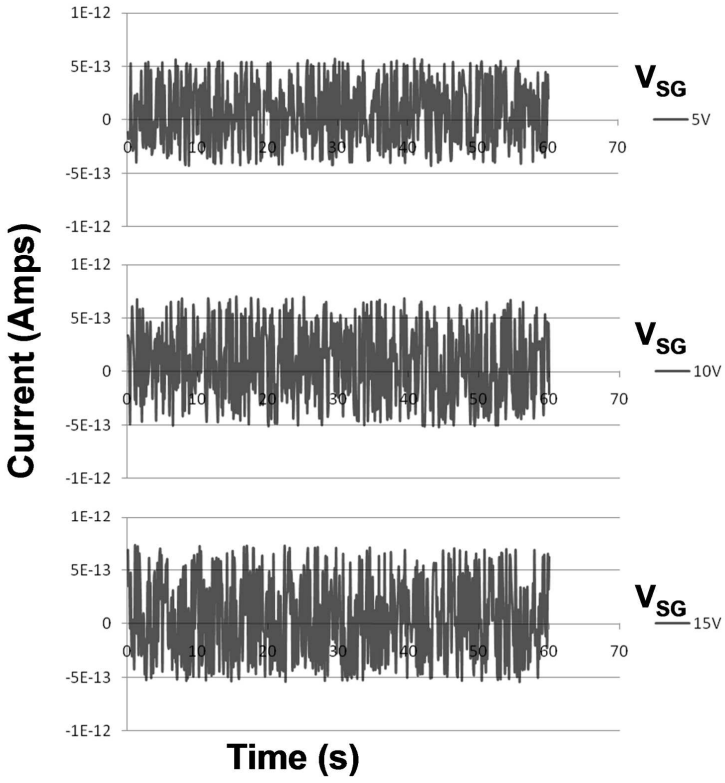

Supplementary Figure 7. Gate leakage current, measured as a function of source-gate voltage (V_{SG}). This data, measured on a nanochannel device with a 10^{-4} M KCl solution, reveals that the gate leakage current contributes negligibly to the nanofluidics transistor (voltage gated current flow) measurements.

References

26. Delgado, A.V. *Interfacial Electrokinetics and Electrophoresis*. (Marcel Dekker, New York, 2002).
27. Lyklema, J. *Fundamentals of Interface and Colloid Science Vol. II*, (Academic Press, London, 1995).
28. Israelachvili, J.N. *Intermolecular and Surface Forces* (Academic Press, London, 1992).
29. Vlassiouk, I., Smirnov, S., Siwy, Z. Ionic Selectivity of Single Nanochannels. *Nano Lett.* **8,** 1978-1985 (2008).